

# Initial interpretation of Titan plasma interaction as observed by the Cassini plasma spectrometer: Comparisons with Voyager 1

R.E. Hartle<sup>a,\*</sup>, E.C. Sittler<sup>a</sup>, F.M. Neubauer<sup>b</sup>, R.E. Johnson<sup>c</sup>, H.T. Smith<sup>c</sup>, F. Cray<sup>d</sup>, D.J. McComas<sup>d</sup>, D.T. Young<sup>d</sup>, A.J. Coates<sup>e</sup>, D. Simpson<sup>a</sup>, S. Bolton<sup>f</sup>, D. Reisenfeld<sup>g</sup>, K. Szego<sup>h</sup>, J.J. Berthelier<sup>i</sup>, A. Rymer<sup>e</sup>, J. Vilppola<sup>j</sup>, J.T. Steinberg<sup>k</sup>, N. Andre<sup>l</sup>

<sup>a</sup>NASA Goddard Space Flight Center, Greenbelt, MD 20771, USA

<sup>b</sup>University of Koln, D 50923 Koln, Germany

<sup>c</sup>University of Virginia, Charlottesville, VA 22904, USA

<sup>d</sup>Southwest Research Institute, San Antonio, TX 78228-0510, USA

<sup>e</sup>Mullard Space Flight Center, Dorking, Surrey RH5 6NT, UK

<sup>f</sup>Jet Propulsion Laboratory, Pasadena, CA 91109, USA

<sup>g</sup>University of Montana, Missoula, MT 59812, USA

<sup>h</sup>KFKI-RMKI, KFKI Research Institute for Particle and Nuclear Physics, Budapest H-1525, Hungary

<sup>i</sup>Centre d'etude des Environnements Terrestre et Planetaires, St. maur-des-Fosses, 94107 France

<sup>j</sup>University of Oulu, Linnanmaa, FIN-90014, Finland

<sup>k</sup>Los Alamos National Laboratory, Los Alamos, NM 87545, USA

<sup>l</sup>CESR, Toulouse, 4346 31028, France

Received 10 November 2005; received in revised form 21 November 2005; accepted 4 May 2006

Available online 14 August 2006

## Abstract

The Cassini plasma spectrometer (CAPS) instrument made measurements of Titan's plasma environment when the Cassini Orbiter flew through the moon's plasma wake October 26, 2004 (flyby TA). Initial CAPS ion and electron measurements from this encounter will be compared with measurements made by the Voyager 1 plasma science instrument (PLS). The comparisons will be used to evaluate previous interpretations and predictions of the Titan plasma environment that have been made using PLS measurements. The plasma wake trajectories of flyby TA and Voyager 1 are similar because they occurred when Titan was near Saturn's local noon. These similarities make possible direct, meaningful comparisons between the various plasma wake measurements. They lead to the following: (A) The light and heavy ions,  $H^+$  and  $N^+/O^+$ , were observed by PLS in Saturn's magnetosphere in the vicinity of Titan while the higher mass resolution of CAPS yielded  $H^+$  and  $H_2^+$  as the light constituents and  $O^+/CH_4^+$  as the heavy ions. (B) Finite gyroradius effects were apparent in PLS and CAPS measurements of ambient  $O^+$  ions as a result of their absorption by Titan's extended atmosphere. (C) The principal pickup ions inferred from both PLS and CAPS measurements are  $H^+$ ,  $H_2^+$ ,  $N^+$ ,  $CH_4^+$  and  $N_2^+$ . (D) The inference that heavy pickup ions, observed by PLS, were in narrow beam distributions was empirically established by the CAPS measurements. (E) Slowing down of the ambient plasma due to pickup ion mass loading was observed by both instruments on the anti-Saturn side of Titan. (F) Strong mass loading just outside the ionotail by a heavy ion such as  $N_2^+$  is apparent in PLS and CAPS measurements. (G) Except for the expected differences due to the differing trajectories, the magnitudes and structures of the electron densities and temperatures observed by both instruments are similar. The high-energy electron bite-out observed by PLS in the magnetotail is consistent with that observed by CAPS.

© 2006 Elsevier Ltd. All rights reserved.

**Keywords:** Titan; Plasma; Pickup ions; Mass loading; Composition; Cassini

\*Corresponding author. Tel.: +1 301 2868234; fax: +1 301 2861663.

E-mail address: [hartle@carioca.gsfc.nasa.gov](mailto:hartle@carioca.gsfc.nasa.gov) (R.E. Hartle).

## 1. Introduction

The complex interaction of Saturn's outer magnetosphere with Titan's atmosphere was observed for the first time by plasma and field instruments when Voyager 1 flew by Titan on November 12, 1980. The initial analysis of the plasma science instrument (PLS) ion and electron spectra by Bridge et al. (1981) found that the rotating magnetosphere was in a subsonic state as it was deflected around Titan, forming a wake through which Voyager 1 passed. The magnetic field measurements by Ness et al. (1981) revealed that Titan does not have an intrinsic magnetic field, but has an induced magnetosphere with a bipolar tail in the wake region. These initial results were followed by the more comprehensive analysis of Hartle et al. (1982, referred to as Paper I), Ness et al. (1982) and Neubauer et al. (1984). Following these early analyses and interpretations, several atmosphere, ionosphere and interaction models (Yung et al., 1984; Yung, 1987; Toubanc et al., 1995; Keller et al., 1998; Ledvina and Cravens, 1998; Brecht et al., 2000) were developed. These models stimulated Sittler et al. (2004, 2005, latter paper referred to as Paper II) to revisit the Voyager 1 data, producing the following: (1) Pickup ions  $H^+$  and  $H_2^+$  dominate at the largest distances from Titan's magnetic tail, followed by  $CH_4^+$  at intermediate distances and  $N_2^+$  just outside the tail. The relative abundance of these ions is consistent with the densities of the corresponding neutral exosphere sources. (2) Exospheric  $CH_4$  and pickup ion  $CH_4^+$  are sources of carbon in Saturn's magnetosphere. (3) Finite gyroradius effects play an essential role in the removal of background magnetosphere plasma by Titan's upper atmosphere. (4) The finite gyroradius effects also implied that the observed hot keV ion component of the ambient plasma is a heavy ion such as  $N^+/O^+$ . (5) A minimum "ionopause" altitude of 4800 km at the subflow point was estimated by a new mass loading approach.

The Voyager 1 and Cassini TA flyby trajectories at Titan are very similar so that direct comparisons of the PLS and Cassini plasma spectrometer (CAPS) plasma measurements are feasible. One similarity is that each flyby trajectory passed through the wake produced by Saturn's rotating magnetosphere plasma as it flows past Titan. Another is the similarity of the solar zenith angles at each flyby, because the TA encounter was  $\sim 10.6$  h LT relative to Saturn and Voyager 1 was  $\sim 13$  h LT. The Cassini flyby trajectory in Titan-centered coordinates is shown in Fig. 1, where the  $y$ -axis points toward Saturn, the  $x$ -axis is in the corotational direction of the rotating magnetosphere and the  $z$ -axis is parallel to Saturn's rotational axis. The Cassini trajectory is super-imposed on the model interaction originally derived by Hartle et al. (1982) from the Voyager 1 data. The "views" in Fig. 1a and b, in the  $-z$  and  $-x$  directions, respectively, show the similarities of the Voyager 1 trajectory to that of the TA encounter, with the exceptions that Voyager 1 is further down the wake and has an almost equatorial pass relative to Cassini's mid-

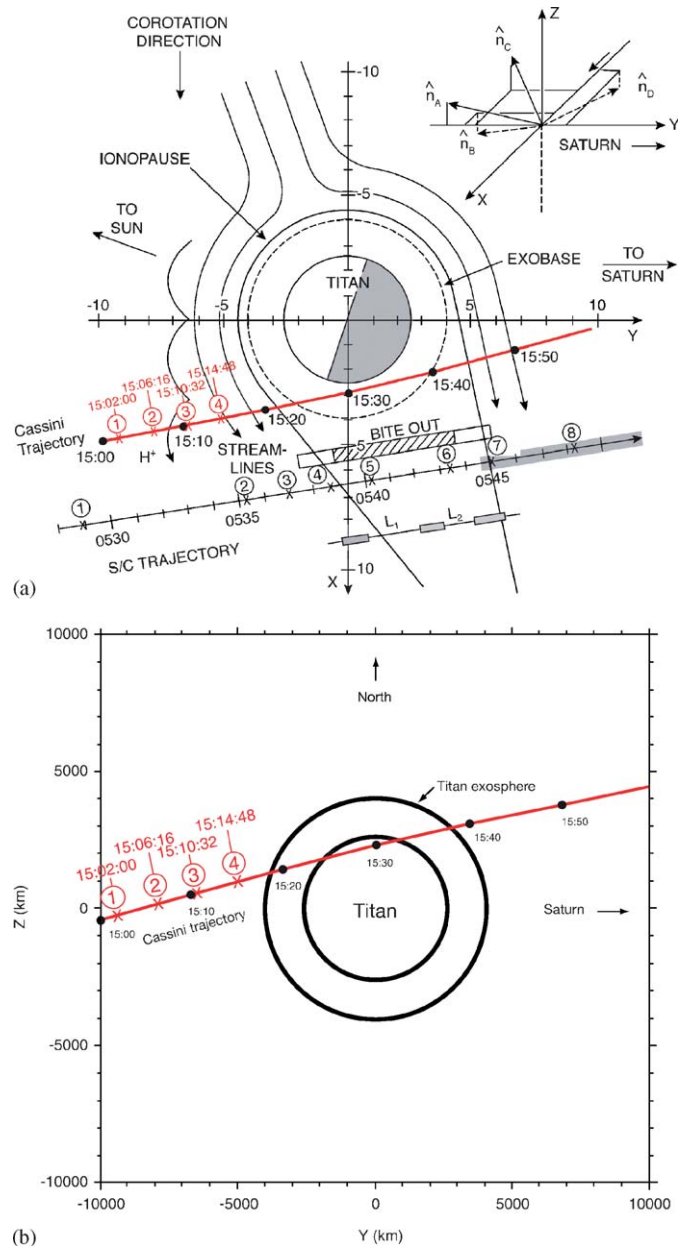


Fig. 1. Geometrical properties of Titan interaction projected onto orbital plane ( $x, y$ ). Spacing on  $x$ - and  $y$ -axes are in intervals of  $10^3$  km. On the Voyager 1 trajectory, the numbers are positions where PLS ion measurements were made, while the CAPS IMS measurements were made almost continuously along the Cassini trajectory. The Voyager 1 trajectory is inclined  $\sim 10^\circ$  to the  $x$ - $y$  plane, while TA is inclined  $\sim 17.3^\circ$ . Voyager 1 crosses the  $x$ - $y$  plane from above at 0542 UT. TA does not cross the  $x$ - $y$  plane in the ionotail; however, for orientation, it crossed the terminator plane above the equatorial plane at 15:29:59 UT. Voyager 1 model exobase and ionopause boundaries from Paper I are shown along with streamline flow and an  $H^+$  pickup ion trajectory (to scale). The inset in the upper right shows the directions of the normal vectors to the four PLS Faraday cups.

latitude pass. For TA, the closest approach altitude was  $\sim 1764$  km from the surface at 15:30:08 SCET (spacecraft event time in [h:min:s] throughout). Voyager 1's closest approach was  $\sim 4400$  km from the surface at 05:40:20 SCET. The model describing the Voyager 1 interaction

shows the neutral exobase, ionopause boundary and the incoming flow, deflected 20° from the corotational direction. The inset in Fig. 1a shows pointing directions of the A, B, C, and D Faraday cups of the PLS on Voyager 1.

The CAPS instrument (Young et al., 2004) is composed of an ion mass spectrometer (IMS), electron spectrometer (ELS) and an ion beam spectrometer (IBS). We will primarily be discussing data from the IMS and ELS. The IBS is most important for Titan’s ionosphere. The IMS covers the ion energy-per-charge range  $1\text{ V} \leq E/Q \leq 50\text{ kV}$  and the ELS has the electron energy range  $1\text{ eV} \leq E \leq 28\text{ keV}$ . Both instruments take simultaneous measurements in collimators divided into eight angular sectors separated by

20° in the collimator plane. The IMS takes singles data ( $E/Q$  spectra), coincident ion data for pre-selected ion species and coincident time-of-flight (TOF) data (or B-cycle data,  $E/Q$  vs. TOF) used for detailed compositional analysis. An IMS energy sweep takes 4 s, the ELS sweep takes 2 s and the B-cycle takes 256 s. For the B-cycle data, we sum 64 energy sweeps and collapse all eight angular sectors for high sensitivity. An actuator sweeps the field of view of the sensors to optimize pitch angle coverage. The actuator was scanned at a rate of  $1^\circ\text{ s}^{-1}$  over a range of  $\sim +107^\circ$  to  $-81^\circ$  during Titan-A, with a sweep across the ram direction for the immediate Titan encounter. The pointing directions of the eight collimators in the IMS

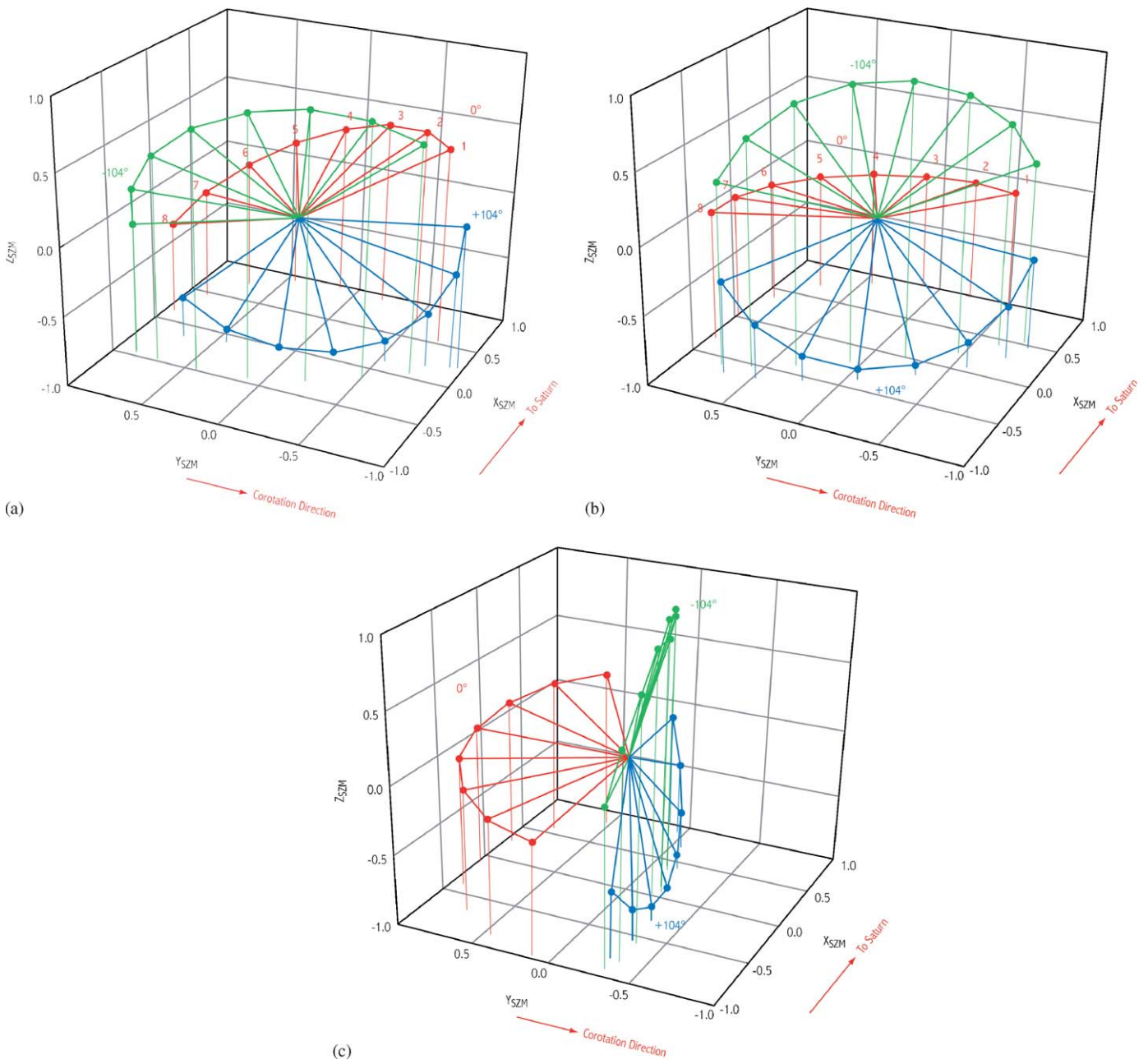


Fig. 2. IMS collimator frame orientation variation as the instruments actuator moves in window washer mode between  $\pm 104^\circ$  of actuator angle. Figs. 2a, b and c correspond to times 13:35:36, 15:14:48 and 17:35:04 SCET. See text for details.

collimator plane for three scan angles of  $104^\circ$ ,  $0^\circ$  and  $-104^\circ$  (note: this represents the nominal scan range that differs from the actual scan used above) are shown at 13:35:36, 15:14:48 and 17:35:04 SCET in Figs. 2a, b and c, respectively. As will become evident below, the earliest and latest time corresponds to regions close to and on either side of the plasma wake, but not in the region where mass loading occurs. The mid-time occurs in the mass loading region described below. Note that the coordinates in Fig. 2 differ from those in Fig. 1, where the  $x$ - and  $y$ -axes of the former are rotated  $90^\circ$  counter clockwise about the  $z$ -axis, which points in the same direction in both figures. The red arrows show that the  $x$ -axis in Fig. 2 points toward Saturn while the nominal corotation vector is in the  $-y$ -direction.

## 2. Ion spectra, flow and composition

Fig. 3 shows Voyager 1 PLS ion distribution functions,  $F$ , vs. energy per charge,  $E/Q$ , observed in the A, B, C and D Faraday cups at the numbered observation points on the trajectory in Fig. 1. We use Figs. 1 and 3 to give a pre-Cassini overview of plasma flow and composition. Simulations of spectra, described in Paper I, revealed background magnetosphere ions  $H^+$ ,  $N^+$  and/or  $O^+$  as indicated. Since the latter two ions were not distinguishable, they were expressed as  $N^+/O^+$  in Paper I. Ions first identified in Paper I are shown in black and those identified in Paper II are in red. Simulations of pickup ion ring distributions derived from model exosphere densities in Papers I and II led to the identification of  $H^+$ ,  $H_2^+$ ,  $N^+$ ,  $CH_4^+$  and  $N_2^+$  ions as shown. As Voyager 1 approached the exobase of Titan, the background  $N^+/O^+$  density decreased considerably because the large  $N^+/O^+$  gyroradii resulted in their penetration of Titan's atmosphere, where they were "absorbed" and lost to the flow. This finite gyroradius

effect described in detail in Paper II did not seem to affect  $H^+$  with its smaller gyroradius. The ion simulations also revealed an increased reduction in the flow velocity as Voyager 1 approached the magnetotail (panels 3–4), slowing to speeds of  $5\text{--}10\text{ km s}^{-1}$  at measurement point 4. The slowing down at point 4 was suggested in Paper I to be due to pickup of the heavy 28 amu ion thought to be  $N_2^+$ . However, a great deal of the slowing down was attributed in Paper II to mass loading by  $CH_4^+$ , because its parent,  $CH_4$ , is the dominant neutral exosphere constituent over most of the slowing down region (see below).

These Voyager 1 PLS observations are now compared with those made by Cassini CAPS, an instrument with a higher time resolution, covers a wider energy range and a TOF capability to identify species mass. We begin with the CAPS  $E/Q$  vs. time spectrogram of IMS "singles", shown in Fig. 4, with all eight angular sectors (note: the striated appearance is a consequence of the scan motion of the actuator). The spectra are termed singles because ion rates are non-coincident and consequently contain no composition information. This spectra has been used in differing formats by Szego et al. (2005), Cray et al. (in review; referred to as Paper III) and Hartle et al. (2006, referred to as Paper IV). All three investigations used time segments of the data differing from Fig. 4 and the first two summed over all angular sectors. The background plasma outside the Titan interaction region has been analyzed by Szego et al. (2005) and Cray et al. (Paper III) and they find that the  $E/Q$  range of plasma outside the Titan interaction region shows up as two peaks with  $E/Q \sim 200\text{ V}$  and  $E/Q \sim 2\text{ kV}$ , consistent with  $H^+$ ,  $H_2^+$ ,  $N^+/CH_2^+$  and  $O^+/CH_4^+$ . In Paper III, Cray et al. found the ions to be flowing at a subrotation speed  $\sim 110 \pm 20\text{ km s}^{-1}$  (corotation speed  $\sim 200\text{ km s}^{-1}$ ) and identified the ion masses above from ion counts vs. TOF data. These composition results

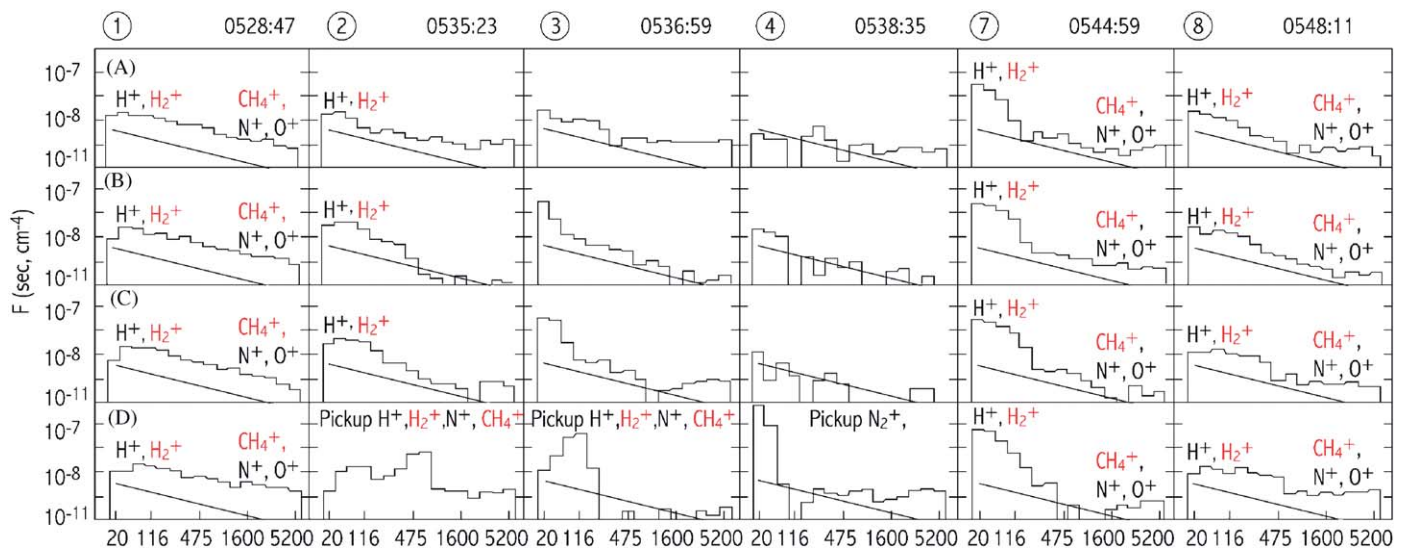


Fig. 3. Ion distribution functions,  $F$ , vs. energy (eV)/charge observed by PLS, where each numbered column corresponds to numbered observation points on trajectory in Fig. 1. A, B, C and D refer to the sensor cups and the slanted lines are the instrument noise levels. Ions are placed above the portions of the distributions they populate, where those identified in Paper I are in black and those of Paper II are in red.

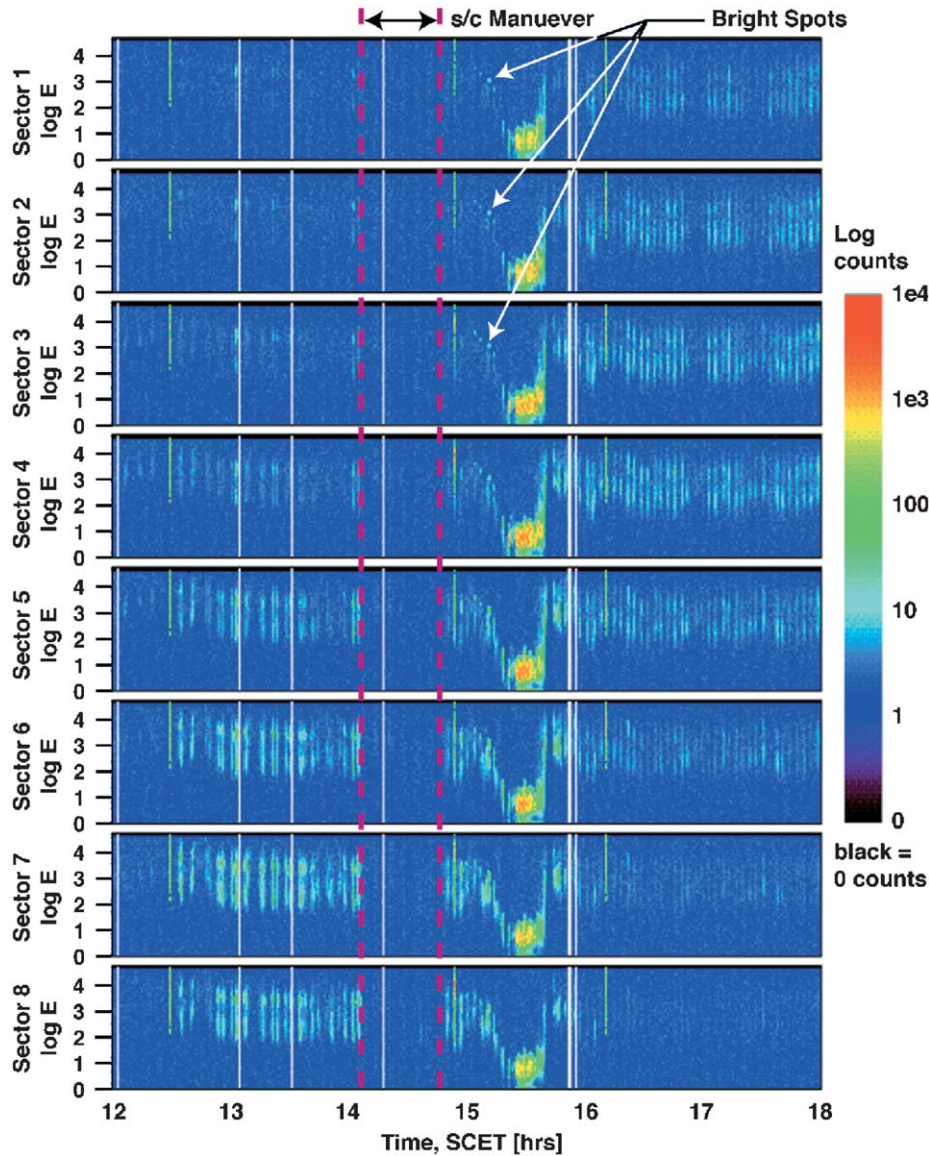
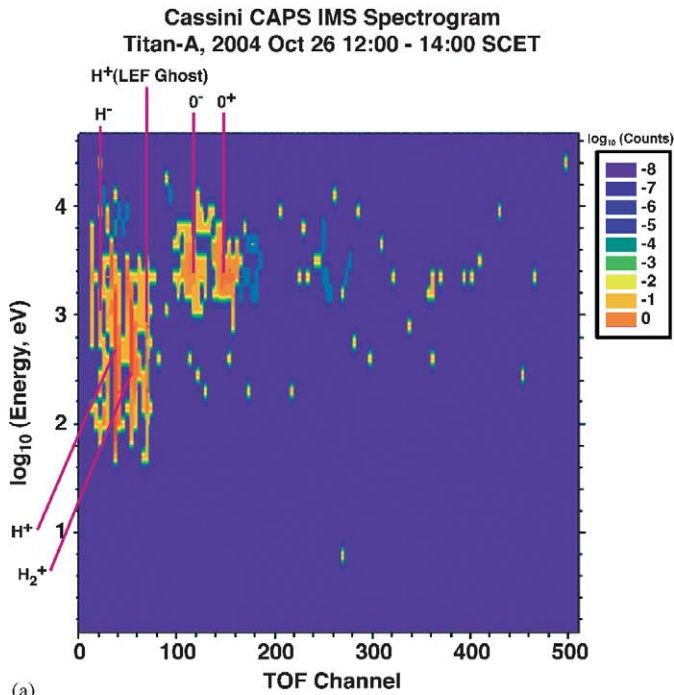


Fig. 4. IMS singles spectrogram observed on TA trajectory. All eight angular sectors are shown as energy per charge,  $E/Q$  (eV) vs. SCET (in [h:min:s] throughout) vs. counts depicted by color scale in logarithmic counts to right. Discrete energy scans appear as vertical swaths. The white vertical lines are data gaps.

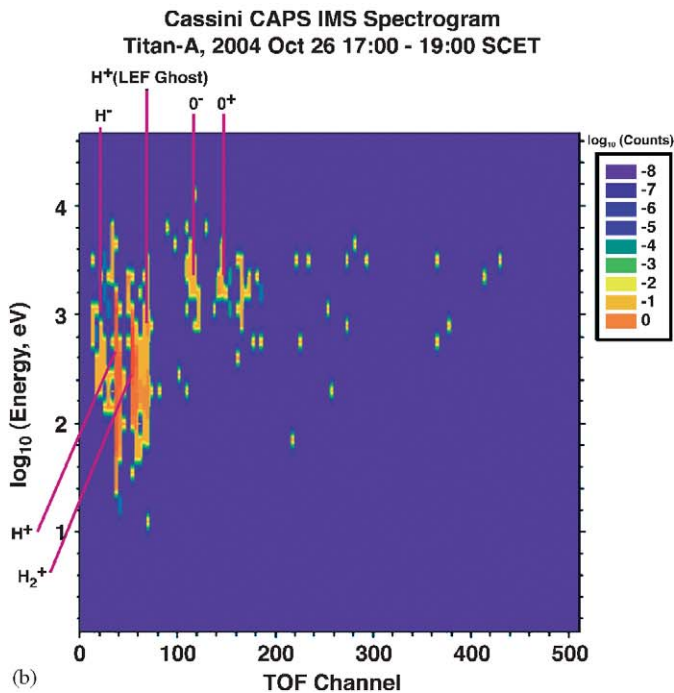
obtained on the anti-Saturn and Saturn facing sides are consistent with the Voyager 1 measurements except that the high data rate of CAPS made it possible to identify  $H_2^+$  in addition to  $H^+$ , and distinguish the 14 amu ion,  $N^+/CH_2^+$ , from the 16 amu ion,  $O^+/CH_4^+$ .

An additional analysis of background magnetosphere ion composition on the ingress and egress legs of TA are made using CAPS  $E/Q$  vs. TOF spectrograms, shown in Figs. 5a and b, respectively. The ingress spectrum is from 12:00 to 14:00 SCET and the egress from 17:00 to 19:00 SCET, both in the vicinity of Titan, but well away from the mass loading regions. During these long observation intervals, counts were integrated over many B cycles. Spectral “lines” for ion masses 1, 2 and 16 amu are identified and interpreted to be  $H^+$ ,  $H_2^+$  and  $O^+$ . This ambient plasma is hot, having energy ranges of  $\sim 0.016$ – $6.3$  keV for  $H^+$ ,  $\sim 0.1$ – $4$  keV for  $H_2^+$  and

$\sim 1$ – $4$  keV for  $O^+$ . The identification of  $H^+$  and  $O^+$  is strengthened by the appearance of  $H^-$  and  $O^-$  lines, their instrumental “fingerprints” (for interpretation of negative ions, see Young et al., 2004). The 16 amu TOF channel may also contain  $CH_4^+$  and the 14 amu TOF channel may signal the presence of  $N^+/CH_2^+$ , all of which were more apparent in the counts vs. TOF analysis in Paper III as described above. Future analysis may clarify such uncertainties in the  $E/Q$  vs. TOF spectrograms. In Fig. 4, the effects of mass loading are depicted by the slowing down of plasma over the period  $\sim 15:00$  to  $\sim 15:18$  SCET. The greatest ion counts from 13:00 to 15:18 SCET appear in the three lowest sectors in Fig. 4, sectors 6 through 8. These sectors correspond to the sector pointing directions of the same numbers in Figs. 2a and b, which are the ones pointing most closely into the corotation direction of the magnetosphere. In the mass



(a)



(b)

Fig. 5. (a) Background or ambient magnetosphere plasma observed on incoming leg of TA by IMS. Coincident TOF color spectrogram shown as function of ion energy per charge,  $E/Q$  (eV), vs. TOF channels with ion counts depicted by the color legend in logarithmic counts to the right. The total number of counts for a given  $E/Q$  are obtained by multiplying the legend by 225, corresponding to the counts from all B cycles between 12:00 and 14:00 SCET. (b) Same as (a) except being for outgoing leg between 17:00 and 19:00 SCET.

loading region, a few “bright spots” (identified by white arrows) near a kV appear in sectors 1 through 4 of Fig. 4, corresponding to pointing directions 1–4 in Fig. 2b. The ions producing these counts have velocity components well away

from the main flow; however, they are consistent with velocities expected of pickup ions traveling in the subrotating plasma depicted in Figs. 1 and 9 below. These signatures are consistent with those expected from narrow beam-like fluxes of heavy pickup ions such as  $\text{CH}_4^+$ , as will be discussed below.

In the mass loading region, the  $E/Q$  range in Fig. 4 decreased from an initial range  $\sim 0.2\text{--}2\text{ kV}$  to  $\sim 5\text{--}50\text{ V}$ , which corresponds to speeds  $\sim 5\text{--}15\text{ km s}^{-1}$  for  $\text{N}_2^+$ , an ion inferred from Voyager 1 PLS measurements (Papers I and II) and suggested by the CAPS TOF data discussed below. This mass loading region, on the anti-Saturn side of Titan, was first identified in Paper I and ascribed to the addition of pickup ion mass by the flowing plasma and momentum exchange between the flowing plasma and pickup ions. The presence of mass loading on the anti-Saturn side of Titan was also discussed briefly in Papers III and IV. At the time of Paper I, only  $\text{H}^+$  and  $\text{N}_2^+$  were thought to be the pickup ions. However, in Paper II, the revised model neutral exosphere, shown in Fig. 6, was used for source calculations of pickup ions. New exosphere species not included in Paper I are  $\text{H}_2$ ,  $\text{CH}_4$  and suprathermal  $\text{N}^*$  (Yung et al., 1984; Yung, 1987; Toublanc et al., 1995; Keller et al., 1998; Michael et al., 2004). They were added in Paper II, including the corresponding ionization rates, to study mass loading due to the five pickup ions  $\text{H}^+$ ,  $\text{H}_2^+$ ,  $\text{N}^+$ ,  $\text{CH}_4^+$  and  $\text{N}_2^+$ . Since then, in situ measurements of the Titan’s neutral atmosphere have been made by Waite et al. (2005) using the Cassini ion neutral mass spectrometer (INMS). The exobase densities used in Fig. 6 (Papers I and II) for  $\text{N}_2$  and  $\text{CH}_4$  were  $10^8\text{ cm}^{-3}$  and  $4 \times 10^7\text{ cm}^{-3}$  while those observed by the INMS are  $3 \times 10^7\text{ cm}^{-3}$  and  $2.5 \times 10^6\text{ cm}^{-3}$ , respectively. The density differences in  $\text{N}_2$  may be due to exobase temperature differences, where those used in Papers I and II were 160 K (obtained from Broadfoot et al., 1981) while those inferred from the INMS were

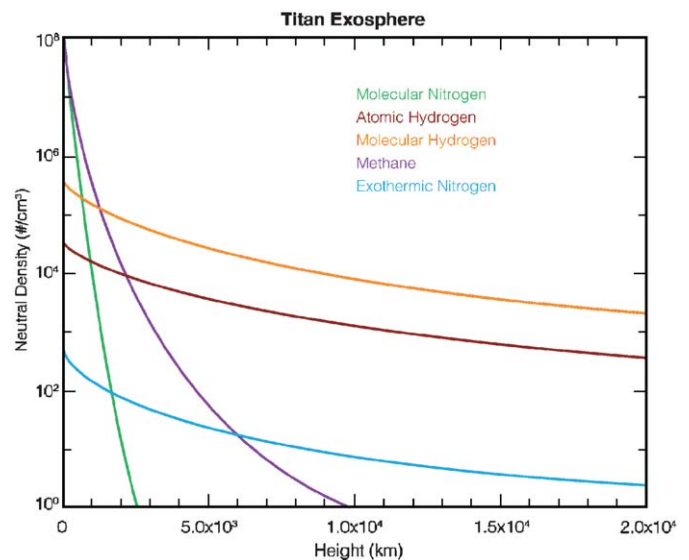


Fig. 6. Titan model neutral exosphere densities vs. height above exobase.

149 K, the atmosphere being cooler and less extended. The differences in the CH<sub>4</sub> densities are much larger and are probably not just due to temperature differences in the atmosphere. We note that the exobase density for CH<sub>4</sub> used in Paper II was derived from a model (see Yung et al., 1984; Yung, 1987) in contrast to the one derived from an actual measurement by INMS.

From 15:22 to 15:40 SCET, the Cassini spacecraft was within Titan's ionotail and passed through the ionosphere, where a vast range of hydrocarbon ions have been identified by the IBS instrument (described in Paper III). A spacecraft maneuver started around closest approach and ended ~16:40 SCET, which changed the pointing of CAPS as indicated by sector pointing in Fig. 2c. The largest counts come from sectors 1 through 4 of Fig. 4, corresponding to sector pointing directions 1 through 4 in the sensor alignments shown in Fig. 2c. As on the inbound leg, these sectors also point approximately into the corotational flow direction. Fig. 4 shows that after 15:40 SCET, the spacecraft exited the ionosphere and quickly returned to the dynamical conditions of Saturn's magnetosphere plasma. This was also the case on Voyager 1's outbound leg (Paper I) as one can see in Fig. 3. That is, in contrast to that on the anti-Saturn side, the rapid recovery is due to the lack of sufficient pickup ions to mass load the plasma. This suggests that the paucity of pickup ions on the Saturn facing side occurs because the cycloidal trajectories of the heavy ions intercept Titan's atmosphere, where most of them are captured. The Cassini magnetometer observed boundaries of the induced magnetosphere between ~15:10 and 15:40 SCET (Backes et al., 2005). These boundaries lie between the mid-mass loading region on the anti-Saturn side and just beyond the ionosphere on the Saturn facing side of Titan.

### 3. Magnetosphere ion erosion by Titan

After further analysis of the PLS ion spectra shown in Fig. 3, it was pointed out in Paper II that, as Voyager 1 approached Titan, the high-energy part of the spectrum disappeared first, which was identified as the heavy component N<sup>+</sup>/O<sup>+</sup> in Paper I. Then the lower-energy component, H<sup>+</sup>, disappeared when the spacecraft was close to the ionopause of Titan. On exiting the magnetotail, the light ion component recovered first followed by the heavy, more energetic component. These variations on both sides of Titan were shown to be finite gyroradius effects in Paper II, where ambient H<sup>+</sup> and N<sup>+</sup>/O<sup>+</sup> are absorbed by the atmosphere on those terminator streamlines whose closest approach distances to the exobase fall inside the ambient gyrodiameters, 800 km and 11,200 km, respectively. Although similar erosion occurs on both anti-Saturn and Saturn facing sides, the combination of the counterclockwise ion gyromotion (Fig. 1 view) and the upstream field of view of PLS and CAPS results in differing signatures on each side of Titan. That is, background O<sup>+</sup> should be observed beyond an ion gyrodiameter from the

exobase on the anti-Saturn side and show no signs of absorption. As one moves inside this distance and the ion orbits cross the exobase, O<sup>+</sup> is expected to diminish as the atmosphere erodes it. On the Saturn facing side of Titan, the same spatial structure of O<sup>+</sup> would be expected if PLS and CAPS had downstream fields of view. Instead, with the instruments facing upstream, the background O<sup>+</sup> is expected to be observed almost immediately upon exiting the ionotail. In this case, the ion gyrocenters are a gyroradius above the exobase. Altogether, at intermediate distances from Titan, finite gyroradius effects are important, while very near the "ionopause", where the flow speeds are low, ~10–15 km s<sup>-1</sup>, the flow is more fluid like. The CAPS data below support these interpretations.

TOF spectrograms in the mass loading region for four B cycle time intervals (~4 min) are shown in Figs. 7a, b, c and d, starting at SCET's: 15:02:00, 15:06:16, 15:10:32 and 15:14:48, respectively. These cycles were briefly discussed in Paper IV and are shown here for completeness and with improved color scales and greater TOF spans. For reference, the Cassini magnetometer observed the beginning of magnetic field draping at ~15:10 SCET (Backes et al., 2005), occurring just before the third B cycle. Spectral signatures of H<sup>+</sup> and H<sub>2</sub><sup>+</sup> along with the accompanying H<sup>-</sup> are identified. The ion energy ranges in the first B cycle, Fig. 7a, are ~0.13–3.4 keV for H<sup>+</sup> and ~0.3–1.2 keV for H<sub>2</sub><sup>+</sup>. Considering the presence of a neutral exospheric source for these ions, their spectra are a mixture of ambient and pickup ions. In contrast, the heavier ion spectra in the range of 14–16 amu are observed in a narrower energy range of ~3.4–4.0 keV. As discussed below, narrow energy ranges or concomitant ion beams are expected for the heavier pickup ions whose gyroradii are much larger than the scale heights of their exospheric source gasses. Of particular interest in this mass loading region is the missing ambient O<sup>+</sup> fingerprint, O<sup>-</sup>, which is consistent with the collisional removal of O<sup>+</sup> by Titan's atmosphere on those magnetosphere plasma flux tubes inside about a gyrodiameter of the Titan's exobase. The concept of removing ambient magnetospheric ions was discussed in Voyager 1 Papers I and II. More recently, it is shown in Paper IV that O<sup>-</sup>, and therefore O<sup>+</sup>, was missing from all B cycles starting at 14:53 SCET (just outside the mass loading region) and extending inward to the B cycle starting at 15:14:48 SCET (just outside the ionopause). The outer distance of this ambient O<sup>+</sup> "clearing region" is ~12,500 km, as measured along the -y-axis (Fig. 1a). The velocity distribution of the ambient O<sup>+</sup> ions are thought to be in a shell velocity distribution. This has been shown to be the case by Szego et al. (2005) through analysis of the 16 amu magnetospheric ions observed by the IMS. Using an MHD model, Ledvina et al. (2005) demonstrated that the ambient heavy ions could be described in terms of a shell distribution. In the clearing region, O<sup>+</sup> has fallen below the detection level of the IMS; however, it must be present at some lower level because some of the O<sup>+</sup> orbits are in transit to the atmosphere before they are absorbed.

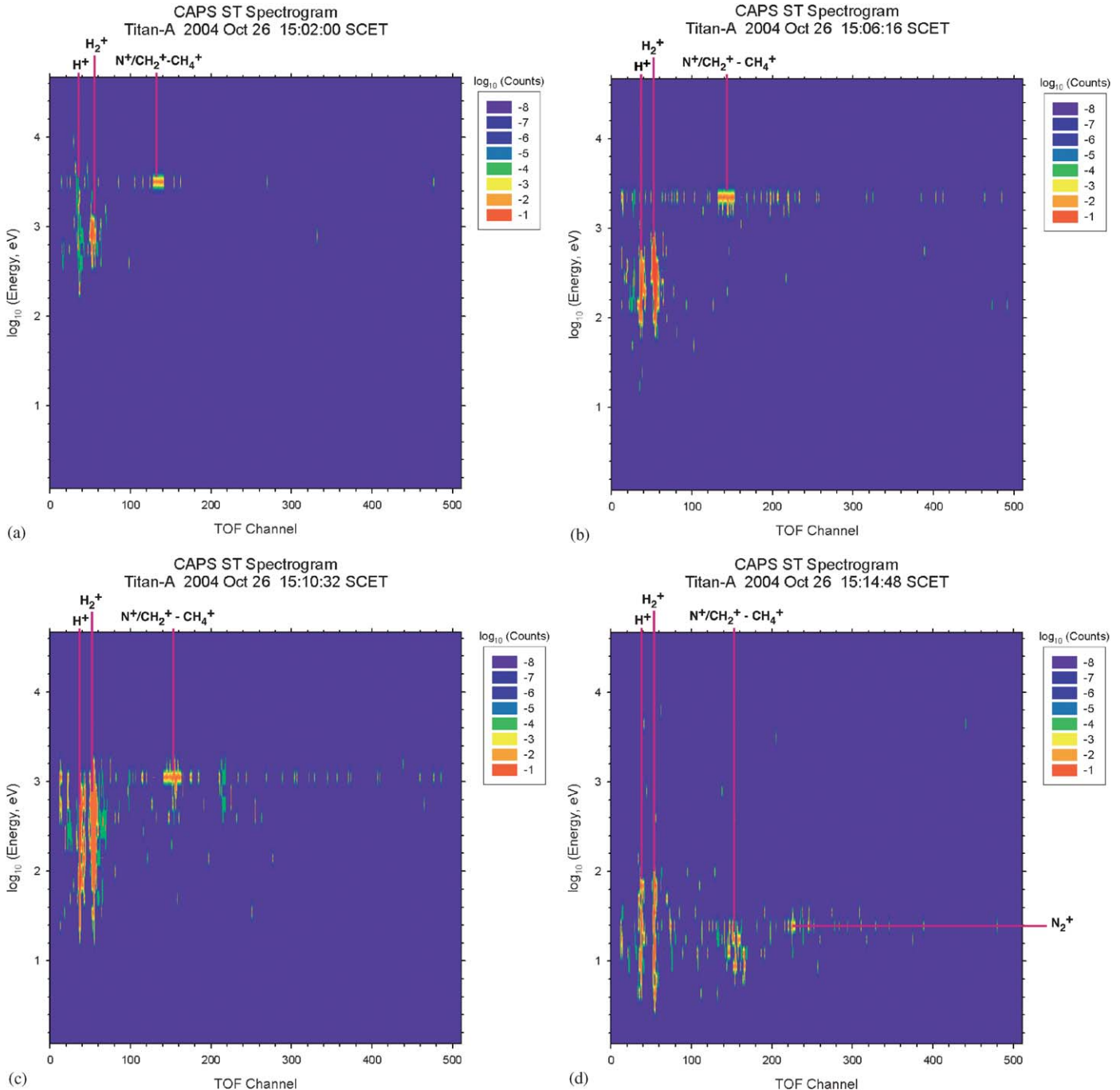


Fig. 7. IMS coincident TOF color spectrogram shown as energy per charge,  $E/Q$  (eV), vs. TOF channels with ion counts depicted by the color legend in logarithmic counts to right. The spectrograms in (a) through (d) are single B cycles observed sequentially in the mass loading region preceding entry into Titan's ionosphere. The total number of counts for each B cycle is obtained by multiplying the numbers in the color legend by 8. The four B cycles (each taking  $\sim 4$  min 16 s) start at SCET's: 15:02:00, 15:06:16, 15:10:32 and 15:14:48, for spectrograms 6a through 6d, respectively.

In the future, it should be possible to estimate the densities of these “ions in transit” using a suitable finite gyroradius model. It follows that the atmosphere should similarly remove any ambient large gyrodiameter ions such as  $\text{N}^+/\text{CH}_2^+$  and  $\text{CH}_4^+$ .

As the above suggests, those ambient  $\text{O}^+$  ions in the magnetospheric plasma flowing past Titan and also penetrating its atmosphere are collisionally removed. In the following, we expand upon a cursory discussion of the

removal rate presented in Paper IV. To estimate the removal rate of the ambient  $\text{O}^+$  ions, we assume the exobase is the highest altitude where collisions are important. Collision rates increase exponentially over relatively thin layers below the exobase because the atmospheric scale height ( $\sim 80$  km, Table 1) is much less than the exobase radius  $\sim 4000$  km. These layers are also thin with respect to an ambient  $\text{O}^+$  ion's gyroradius of  $\sim 4250$ . The observed outer boundary of the  $\text{O}^+$  clearing

Table 1

Ion gyroradius,  $r_g$ , and neutral gas scale height at exobase,  $H$ , are in km

Pickup ion length	H <sup>+</sup>	N <sup>+</sup>	CH <sub>4</sub> <sup>+</sup>	N <sub>2</sub> <sup>+</sup>
$r_g$	191	2680	3060	5360
$H$	2185	156	137	78
$r_g/(H)$	0.087	17.2	22.4	68.7

The parameters used to obtain these values here and throughout are the following: background speed,  $V_b = 110 \text{ km s}^{-1}$ ; magnetic field,  $B = 6 \text{ nT}$  (Backes et al., 2005); exobase temperature  $T = 149 \text{ K}$  (Waite et al., 2005).

region of  $\sim 12,500 \text{ km}$  can be used to estimate the ambient O<sup>+</sup> ion gyrodiameter by subtracting the exobase radius of  $4000 \text{ km}$  to obtain a gyrodiameter of  $8500 \text{ km}$  or a gyroradius of  $4250 \text{ km}$  with a guiding center at  $y = -8250 \text{ km}$ . This empirical estimate of the ambient gyrodiameter is considered a lower value because the more energetic O<sup>+</sup> ions in the velocity distribution that are removed from the flow would have larger gyrodiameters. Because the ions are in a shell distribution, the corresponding depth of penetration in the collisional region should be thin relative to that of broader Maxwellian distributions.

The ambient O<sup>+</sup> ions that penetrate the atmosphere move toward Titan from above and below as they travel along magnetic flux tubes flowing past Titan. The ions must also move in the  $x$ -direction on guiding centers bounded by  $|y| < 8250 \text{ km}$ . This outer boundary is outside the distance where any noticeable deflection of magnetospheric flow around Titan has been observed [e.g., the first indication of field line draping occurred at  $\sim 15:10 \text{ SCET}$  (Backes et al., 2005) and slowing down begins after Fig. 7a)]. As the ambient ions move along a magnetic flux tube toward Titan, they have a velocity component along the magnetic field and one in the rotational direction ( $+x$ -direction of Fig. 1a). The guiding center velocity in the  $x$ -direction is the rotational flow speed of  $110 \text{ km s}^{-1}$ . We assume that about half of the ions above the equatorial plane move downward with speeds near the thermal speed. A conservative estimate for this speed is the bulk flow speed,  $110 \text{ km s}^{-1}$ , since the background plasma is subsonic. Combining the components in the  $x$ - and  $y$ -directions, the total speed of an ion moving toward Titan would then be  $\sim \sqrt{3/2} \times 110 \text{ km s}^{-1} = 135 \text{ km s}^{-1}$ , where a pitch angle of  $45^\circ$  was assumed. In this case, the downward flux of ambient O<sup>+</sup> ions is  $\sim 4 \times 10^5 \text{ cm}^{-2} \text{ s}^{-1}$ , using half of the observed density (Paper III) of  $0.06 \text{ cm}^{-3}$ . The outer boundary of the effective area where collisions with the atmosphere can occur is approximated by the circular cross section of radius  $8250 \text{ km}$ , the maximum guiding center position of an O<sup>+</sup> ion reaching the exobase. Thus, the effective area or clearing area is  $\sim 1.2 \times 10^{18} \text{ cm}^2$ . The net loss rate of ambient O<sup>+</sup> is then  $\sim 9.5 \times 10^{23} \text{ s}^{-1}$ , accounting for the fluxes from above and below. This value needs to be adjusted downward because a fraction of the ions in the flow do not reach the exosphere because the ion gyration time is greater than the time it takes a magnetic flux tube to flow across the collision area. It can be shown

that the average time collisions are occurring in the collision region (time is larger near the equatorial region and vanishes at the poles) as a magnetic flux tube flows through the region is  $\langle t_c \rangle \sim 104 \text{ s}$ . Since the gyroperiod of an ambient O<sup>+</sup> ion is  $t_g \sim 175 \text{ s}$ , the effective fraction of the density that actually collides with the atmosphere is  $104/175 = 0.59$ , yielding a net loss rate of  $\sim 5.6 \times 10^{23} \text{ s}^{-1}$ . This value is about 37% less than the one obtained in Paper IV, which used a somewhat different approach and did not correct for the average collision times. Because of the complexity of the interaction region, more accurate loss rates will require a 3D kinetic model or its equivalent. Furthermore, because of the temporal variability of the environment around Titan, more ion measurements are needed to obtain an improved picture of the O<sup>+</sup> clearing region.

#### 4. Pickup ions and their distributions

As described in Paper I, the newly born pickup ions are accelerated by the motional electric field,  $\mathbf{E} = -\mathbf{V} \times \mathbf{B}$ , pointing away from Titan when in Saturn's equatorial plane, where  $\mathbf{V}$  is the background velocity of Saturn's rotating magnetosphere and  $\mathbf{B}$  is its magnetic field. In the region outside magnetic field draping, the ions move in a plane perpendicular to  $\mathbf{B}$ , which is also perpendicular to the plane containing both  $\mathbf{V}$  and  $\mathbf{B}$ . Their distribution in velocity space is two-dimensional and referred to as a ring distribution. At distances well away from Titan, newly born pickup ions move in cycloidal trajectories in planes approximately parallel to Saturn's equatorial plane (ions born at essentially zero velocity relative to background speed). As the magnetic field begins to drape around Titan, these planes begin to tilt from the equatorial plane. The field was observed to start draping at  $\sim 15:10 \text{ SCET}$  (Backes et al., 2005), just before the B cycle of 7c. The draping becomes more prominent during the B cycle of 7d. Thus, the ions traveling between the third and fourth B cycles will move on surfaces out of the equatorial plane, which tend to be perpendicular to the magnetic field. In particular, newly born ions move perpendicular to the instantaneous plane containing both  $\mathbf{V}$  and  $\mathbf{B}$ , while previously born, energetic ions tend to stay closer to their plane of origin.

Inside the heavy ion background erosion region, we identify the remaining 14–16 amu ions as pickup ions, where the 16 amu ion is identified as CH<sub>4</sub><sup>+</sup> since methane is the dominant 16 amu exospheric constituent (Paper II) as seen in Fig. 6. The mass 14 amu pickup ion could be a mixture of N<sup>+</sup> and CH<sub>2</sub><sup>+</sup>, where the former is the dominant 14 amu exospheric gas and the latter ion is a fragment of its parents CH<sub>4</sub> and CH<sub>4</sub><sup>+</sup>. Another 28 amu ion, HCNH<sup>+</sup>, identified as a possible dominant ionospheric ion in Paper I, and confirmed by the Cassini INMS (Kasprzak, private comm.), has also been suggested as a possible ion in the mass loading region. If this is the case, it implies that some of the plasma in Fig. 7d is of ionospheric origin. These ions

would then have been scavenged by the interaction of the externally flowing plasma with the ionosphere, a well-known process observed at Venus.

Light constituent pickup ions such as  $H^+$  and  $H_2^+$  can be identified by the abrupt drop in the energy distributions at the pickup ion cutoff energies (maximum possible energy at maximum ion speed of  $2 \times$  the ambient plasma flow speed) However, when the ion gyroradii exceed the scale heights of their neutral source gasses, the ions can no longer be identified by such cutoff energies. This is demonstrated by the ion flux distributions shown in Fig. 8, which are plots of analytic solutions to the Vlasov equation (Hartle and Sittler, 2004). This analysis clearly shows that the ratio of a pickup ion's gyroradius,  $r_g$ , to its source scale height,  $H$ , is a fundamental parameter in determining the nature of its velocity distribution as can be realized from the corresponding ratios in Table 1. The figure shows pickup ion flux distributions for exponential neutral exosphere sources that increase along the  $x$ -axis. A uniform magnetic field is in the  $z$ -direction (see inset), the background velocity is in the  $x$ -direction and the motional electric field is in the  $y$ -direction. The distribution functions,  $f$ , have been normalized by  $2r_g RN_0/V_b^3$ , the product of their respective gyroradii, ion production rates and neutral densities (at the observation point) divided by the cube of the background speed. The component velocities are normalized by the background speed,  $V_b$ . The velocity space geometry defines the total velocity,  $V$ , and the corresponding velocity,  $v$ , in the moving frame at an angle  $\theta$  to  $V_x$  (i.e.,  $x$ -axis along direction of ambient flow). The gyroangle  $\theta$  has the range  $-\pi$  to  $\pi$ , where pickup ions are born with vanishing velocity at  $\theta = \pi$ , attain their maximum velocity at  $\theta = 0$  and return to zero velocity at  $\theta = -\pi$ . In the source region, the flux distributions of the light species are relatively strong up to their cutoff energies while the heavy constituent fluxes, with  $r_g/H \gg 1$ , are only strong at low total velocities and  $\theta$

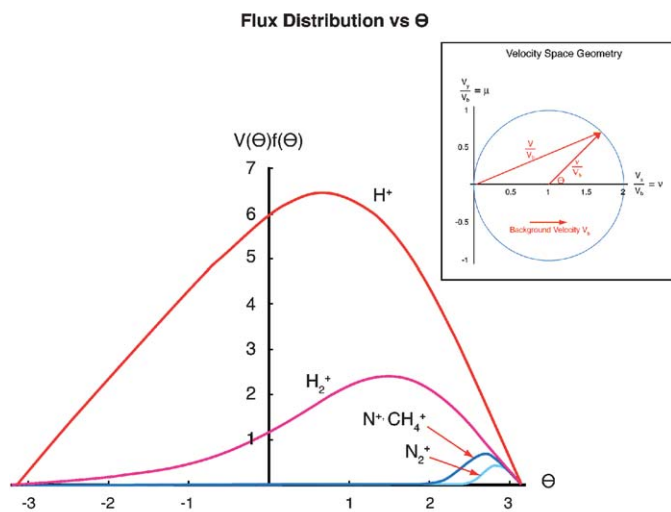


Fig. 8. Flux distributions  $Vf$  vs.  $\theta$  (radians), where  $f$  is normalized by  $2r_g RN_0/V_b^3$ . Velocity space geometry is shown in the inset and described in the text. The pickup ion gyroangle  $\theta$  range is  $-\pi$  to  $\pi$ .

near  $\pi$ . The latter result indicates that the heavy ions have only traveled a short distance from birth  $x \sim H \ll r_g$ , up to about a scale height away. When away from field line variations or draping, the beam like nature of the heavy ions in the source region continues downstream, beyond the source, with higher energy flux peaks distributed on cycloidal trajectories.

To further illustrate why an ions velocity distribution is dependent on the ratio of its gyroradius to the source gas scale height and why  $CH_4^+$  should be observed as a narrow beam, consider the  $CH_4^+$  pickup ion trajectories shown in Fig. 9. The cycloidal pickup ion trajectories are drawn to scale (using the parameters of Table 1), where the ions are born at zero velocity on the line of origins (see Hartle and Killen, 2006), assuring that they all pass through the observation point, O, on the TA trajectory. This approximate example assumes that the pickup ion trajectories are shown moving at sufficient distances outside the interaction region where the background plasma is flowing uniformly. The outer boundary of the interaction region is approximated by the point on TA where magnetic field draping is first observed at  $\sim 15:10$  SCET (Backes et al., 2005). Although the cyan curve in Fig. 9 passes through this point, the projection of points beyond it is only intended to illustrate that there is some boundary beyond which the background plasma flows uniformly. Similarly, an approximation to the ionopause is also shown, where it is drawn to pass through the ionopause at  $r \sim 4600$  km (estimated in Paper II) at the subflow point and also the

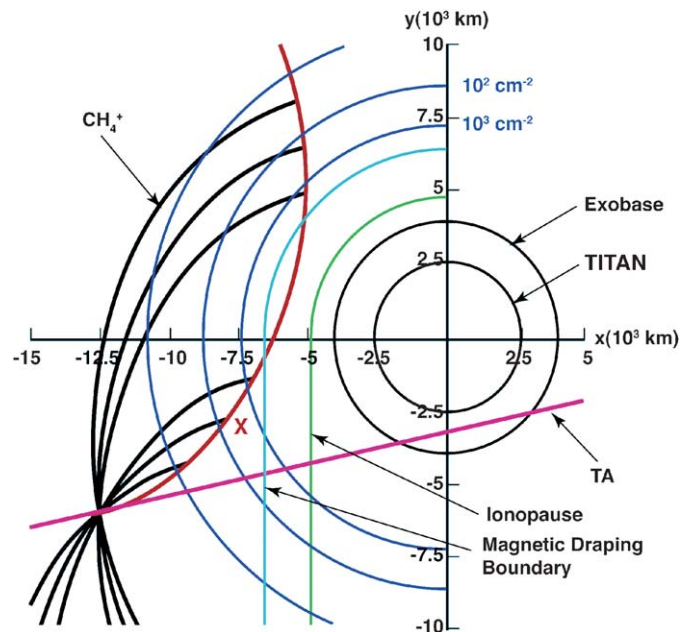


Fig. 9.  $CH_4^+$  pickup trajectories (black) born with zero velocities on the line of origins (red) that assures they pass through the observation point, O, on the Cassini TA trajectory (magenta). Titan and the exobase are shown in black while ionopause and magnetic draping boundaries are sketched in green and cyan, respectively. The blue lines correspond to decadal variations of  $CH_4$ , where the innermost level is  $\sim 10^3 \text{ cm}^{-2}$  from model of Sittler et al. (2005).

point on TA where cool ionospheric electrons are first observed (Coates et al., 2005). The blue lines correspond to decadal variations of  $\text{CH}_4$ , where the innermost level is  $\sim 10^3 \text{ cm}^{-2}$  from the model of Paper II. We note that the outer boundaries of the mass loading region (background slowing down region) and the field draping region begin on about the same boundaries. Because the background plasma inside these boundaries moves more slowly than outside, the ions born within these boundaries will not be accelerated as fast as in the uniform flow region outside and consequently will not reach as far as the observation point, O. In this case, the pickup ions born just outside about the first scale height beyond the slowing down region will arrive at the observation point with the largest fluxes, since they come from points with the largest  $\text{CH}_4$  densities and  $\text{CH}_4^+$  production rates. The energy of an ion accelerated in the motional electric field over a distance  $L$  ( $10^3 \text{ km}$ ) in the  $-x$ -direction from birth place to the observation point, O, will have an energy  $\sim 0.66L$  (kV). The  $\text{CH}_4^+$  energies observed in the region surrounding O are similar to those in Figs. 7a and b. Therefore, if the peak energy is  $\sim 3 \text{ kV}$ , then  $L \sim 4.5 \times 10^3 \text{ km}$ . This distance traced backward on a trajectory from O corresponds to a position  $x \sim -8 \times 10^3 \text{ km}$  and  $y \sim -2.5 \times 10^3 \text{ km}$  on the line of origins. This trajectory is identified by a red X on the line of origins in Fig. 9. In this case, the bulk of the ions observed at O are likely to have been born along the line origins from X outward to the point where  $\text{CH}_4$  has decayed one or two scale heights. Referring to Fig. 6, the scale height of  $\text{CH}_4$  is  $\sim 700 \text{ km}$  at point X. The energy variation of ions at O born over one or two scale heights near X is  $\sim 0.5\text{--}1 \text{ kV}$ . This narrow energy range is similar to the peak widths of the  $\text{CH}_4^+$  pickup ions in Figs. 7a and b. This semi-quantitative example is only intended only to illustrate that when the gyroradius exceeds the ion source scale height, the resulting energy distribution is a narrow beam. Further data analysis and modeling are needed to quantify this picture.

As mentioned above, newly born ions move perpendicular to the instantaneous plane perpendicular to the  $\mathbf{V}\text{--}\mathbf{B}$  plane, while previously born, energetic ions tend to stay closer to their plane of origin. In the pickup region, the dominant heavy ions,  $\text{N}^+/\text{CH}_2^+$ ,  $\text{CH}_4^+$  and  $\text{N}_2^+$ , have values of  $r_g/H \gg 1$  (Table 1). Consequently, considering the above, the observed distributions will span a narrow velocity range, with peaks populated with ions born over the range of an atmospheric scale height. Similarly, upon entering the field line draping region, some additional spread in the ion beam will occur; however, since  $r_g/H \gg 1$ , the space and energy spread will not be large because the ions were born over a length scale  $\sim H$ , relative to their gyroradii,  $r_g$ . The spread will only become large when the scale length for magnetic field variations is much less than the atmospheric scale height, which is not the case in the ion pickup region (see Backes et al., 2005).

We use the actuator motion of the IMS in the mass loading region to aid in identifying pickup ion distribu-

tions. As the actuator continuously sweeps about  $100^\circ$  above and below the equatorial plane, the collimator should accept pickup ions over a segment of its angular sweep. If the ions were not confined to the narrow beams described above, they would be observed over wider angular swaths of the collimator. The spectra of the 14–16 amu ions in Fig. 7 appear to be consistent with the signatures of pickup ions in narrow beam distributions. Furthermore, the pickup ion energies “jump” to lower energy ranges on passing from Figs. 7a–d, corresponding to four separate B cycles. Such jumps are expected for a beam-like distribution because the collimator (see collimator angles in Fig. 10 below) makes only one complete pass during each B cycle, assuring the likelihood that an ion beam would be crossed. The energy jump occurs because the plasma speed continuously decreased during each B cycle while the distribution is only observed during a short portion of the cycle when the collimator can accept ions in the beam, which is a point where the background plasma speed is less than that of the preceding B cycle. Other distributions, such as a shell distribution, would have broader velocity spectra observed over larger collimator scan angles, permitting the effects of more plasma deceleration to be included.

## 5. Mass loading

Mass loading was qualitatively identified in the singles data of Fig. 4 and made more realistic with the identification of pickup ions through analysis of the TOF data in Fig. 7, which can also be used quantitatively to study the slowing down properties. For example, passing from Figs. 7a–c, there is a gradual decrease in the ion energies of about 1.5 to 2 times in the 14–16 amu range, respectively. However, as Cassini moved even closer to Titan, passing from Fig. 7c,d, there is a significantly greater energy drop of 125 times in these ions. Such a large energy decrease can be attributed to at least two factors, an increase in the density (or production rate of the ions) and mass of the pickup ions born upstream. Referring to the exosphere profiles of Fig. 6, one can see that this is likely to be the case; i.e., there is a rapid increase in the neutral source gas densities as the distance to Titan decreases. Furthermore, the rapid increase is due to the heavier constituents,  $\text{CH}_4$  and  $\text{N}_2$ , where the latter (with shorter scale height  $\sim 85 \text{ km}$ ) becomes dominant as the exobase is approached, which is consistent with Fig. 6 and confirmed by the recent INMS measurements (Waite et al., 2005) described above. All of this is consistent with our initial identification of the 28 amu ion as  $\text{N}_2^+$ , with flow speeds  $\sim 10\text{--}15 \text{ km s}^{-1}$ , and its appearance in the last B cycle observation, which is just before entering the cooler, denser ionospheric plasma observed by Coates et al. (2005), bounded by an ionopause-like boundary. This also supports the mass loading picture inferred from the PLS observations on Voyager 1 (Paper I), where  $\text{N}_2^+$  was also thought to be the heavy mass loading ion producing very

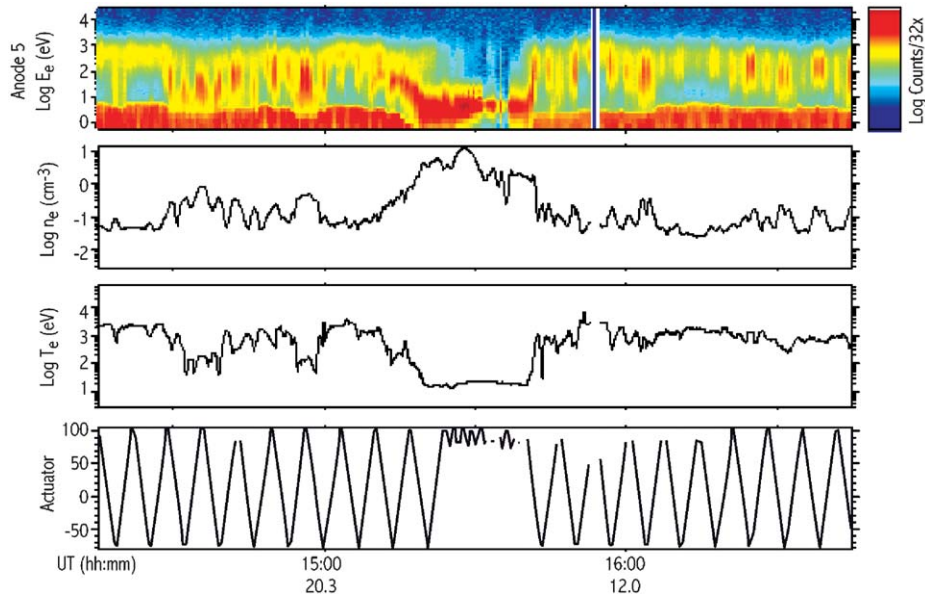


Fig. 10. Electron properties from ELS observations. Top panel: electron energy vs. SCET vs. count rate (color scale in logarithmic counts to right); second from top: electron density,  $n_e$ , vs. SCET; third from top: electron temperature,  $T_e$ , vs. SCET; fourth from top: actuator scan angle above and below equatorial plane at  $0^\circ$ .

low speeds just outside the ionopause. Furthermore, the model calculation in Paper II obtained flow speeds of the background plasma that also supported the mass loading picture described in Paper 1 and above.

### 6. Electron measurements

Electron energy count rates, densities, temperatures and scan angles obtained from the Cassini ELS are shown as a function of SCET in Fig. 10. The densities and temperatures have a number of similarities to those observed by PLS on Voyager 1 (Paper I), as shown in Fig. 11a. For example, both show a buildup of density as Titan is approached. On entering the ionosphere on the inbound leg, ELS densities continue to increase, reaching a peak in the ionosphere. No such peak appeared in the PLS measurements because Voyager 1 was in the magnetotail (we refer to an ionotail as that part of the tail within the ionosphere while further downstream we call it a magneto-tail), far from the ionosphere. On the inbound and outbound legs of Voyager 1 and Cassini, but well beyond the ionotail, both ELS- and PLS-derived electron densities are similar at  $\sim 0.1 \text{ cm}^{-3}$ . The corresponding ELS electron temperatures ranged between  $\sim 100$  and  $\sim 1000 \text{ eV}$ , being higher than the  $\sim 200 \text{ eV}$  observed by PLS. The electron velocity distributions observed by the Voyager 1 PLS in the wake region (Paper I) are shown in Fig. 11b. A unique feature of these distributions is the electron depletion or “bite-out” in the electron spectra above  $700 \text{ eV}$ . The electron bite-out of energetic magnetospheric electrons observed by the PLS is also seen in the flux spectrum of the ELS. The bite-out was interpreted in Paper I to be due to

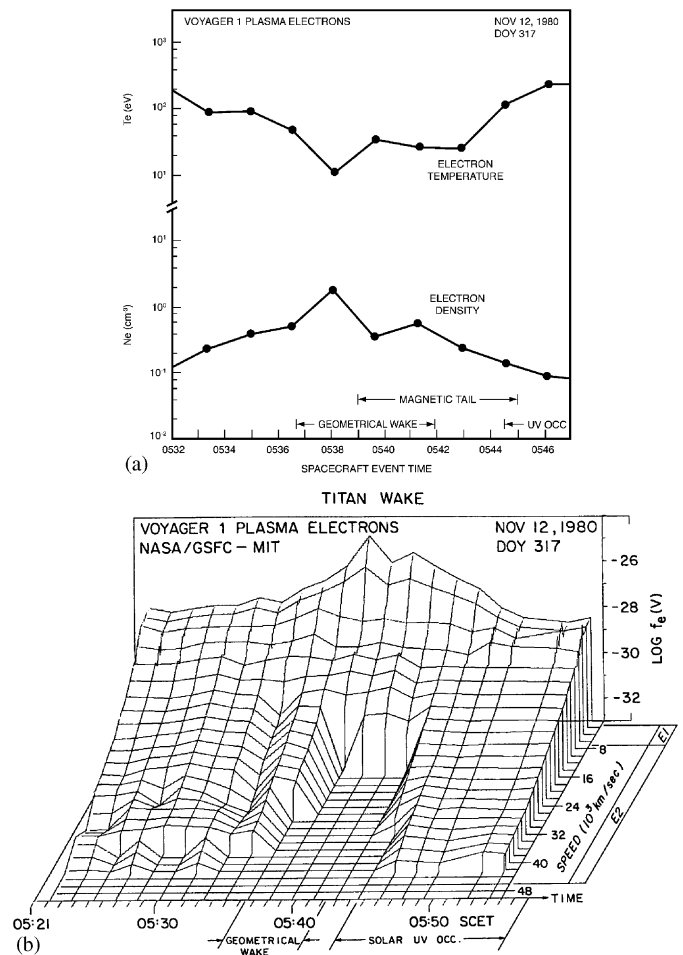


Fig. 11. (a) Voyager 1 electron densities and temperatures vs. SCET. (b) Electron distribution function vs. electron speed vs. SCET.

scattering down in energy of Saturn's magnetospheric electrons by Titan's neutral atmosphere through which the draped magnetic field lines thread. Electron cooling on Voyager 1's inbound approach to the magnetotail is consistent with the addition of cool photoelectrons during pickup ion formation. Such cooling is observed by ELS as Cassini moved into the more dense ionosphere. The resulting density buildup is consistent with the addition of pickup ions and the corresponding slowing down due to mass loading. These features are absent on Voyager 1 and Cassini as they exit the ionosphere on their outbound legs, which is consistent with the decreased formation of pickup ions on the Saturn facing side of Titan. We note that the Voyager 1 electron spectrum was reproduced rather well by the model of Gan et al. (1992) and should be applicable to the Cassini measurements due to the similarities in the PLS and ELS observations.

## 7. Summary

The fortuitous similarities of the plasma wake trajectories of the Cassini TA and Voyager 1 flybys, occurring near Saturn's local noon, made it possible to make direct, meaningful comparisons of the plasma observations made by CAPS and PLS. In general, the features of the interaction of Saturn's rotating magnetosphere with Titan's atmosphere observed by the two instruments were found to be similar. In each case, the background magnetospheric plasma in the vicinity of Titan was observed to be subsonic, where a speed of  $110 \text{ km s}^{-1}$  (subrotation) was inferred from CAPS measurements. On the anti-Saturn side, the slowing down of magnetospheric plasma observed by the PLS was also found to be the case for the CAPS measurements. Each instrument observed the plasma to slow down at an increasing rate as the ionopause was approached. During the Cassini TA flyby, the plasma slowed down from  $\sim 110$  to  $\sim 10\text{--}15 \text{ km s}^{-1}$ . In Paper I, the slowing down was attributed to mass loading by pickup ions born from the extended exosphere. The principal pickup ions,  $\text{H}^+$ ,  $\text{H}_2^+$ ,  $\text{N}^+$ ,  $\text{CH}_4^+$  and  $\text{N}_2^+$  were inferred from the PLS measurements (Papers I and II) and confirmed by CAPS observations. The latter observations made ion identification more definitive due to the TOF capability as well as having higher data rates than Voyager 1. The heaviest of the pickup ions,  $\text{CH}_4^+$  and  $\text{N}_2^+$ , appear to do most of the mass loading, as suggested in the model of Paper II. The B cycle,  $E/Q$  vs. TOF, measurements of Fig. 7 showed that the heavy pickup ion distributions can be interpreted in terms of narrow energy ion beams as expected from ions whose gyroradii are much larger than the source gas scale height. Although the 28 amu pickup ion has been identified as  $\text{N}_2^+$ , one might question the possible presence of the ionospheric ion,  $\text{HCNH}^+$ , which may have penetrated the ionopause and joined the downstream flow of pickup ions. Additional flyby measurements and further analysis of the fragments in the IMS may shed light on this question.

Ambient magnetosphere  $\text{O}^+$  was observed to be removed from the flow by the IMS on CAPS. Such a clearing zone for the ambient magnetosphere was initially identified using Voyager 1 observations, where magnetospheric ions such as  $\text{O}^+$  are collisionally removed by Titan's upper atmosphere. The dimension of the  $\text{O}^+$  clearing area is about an ion gyrodiameter,  $\sim 8500 \text{ km}$ , above the exobase, as measured in the ion's plane of gyration. This oxygen source (water ions may also be present) could be an important source of oxygen–water to Titan's atmosphere. The oxygen could be locked up in the reducing atmosphere of Titan in the form of CO (Lutz et al., 1983),  $\text{CO}_2$  (Samuelson et al., 1983) and water vapor (Coustenis et al., 1998). Another important source of water and oxygen to Titan's atmosphere is micrometeorites (Samuelson et al., 1983). But, the CO in Titan's atmosphere could also be primordial (Owen, 1982). As the properties of the ambient magnetosphere change, the characteristics of the clearing area will change. Observations from future flybys may make it possible to obtain parametric relationships between the two regimes.

A number of similarities were found in the PLS and ELS electron measurements during their flybys of Titan. For example, well outside the ionotail, the electron densities were observed to be similar at  $\sim 0.1 \text{ cm}^{-3}$ , while the PLS electron temperature of  $\sim 200 \text{ eV}$  was within the broader range,  $\sim 100$  to  $\sim 1000 \text{ eV}$ , observed by the ELS. Furthermore, both instruments observed a buildup of electron density as Titan is approached. Both Voyager 1 and Cassini electron instruments observed the presence of a high-energy electron bite-out inside the ionopause boundary. The bite-out is due to the scattering down in energy of magnetospheric electrons, on draped field lines, as they collide with Titan's upper atmosphere, leaving behind photoelectrons and secondary electrons produced at energies predominantly less than  $\sim 10 \text{ eV}$ . When future flybys cut through the magnetotail at a distance from Titan similar to that of Voyager 1, meaningful comparisons of ELS and PLS electron properties should be possible. In this case, the position of Titan should be close to Saturn noon, as with the Cassini TA flyby.

## References

- Backes, H.F., et al., 2005. Titan's magnetic field signature during the first Cassini encounter. *Science* 308, 992.
- Brecht, S.H., Luhmann, J.G., Larson, D.J., 2000. Simulation of the Saturnian magnetospheric interaction with Titan. *J. Geophys. Res.* 105, 13,119.
- Bridge, H.S., et al., 1981. Plasma observations near Saturn: initial results from Voyager 1. *Science* 212, 217.
- Broadfoot, A.L., et al., 1981. Extreme ultraviolet observations from Voyager 1—encounter with Saturn. *Science* 212, 206.
- Coates, A.J., et al., 2005. Cassini's first Titan encounters: a comparison of plasma results. *Geophys. Res. Abstracts* 7, 08841.
- Coustenis, A., Salama, A., Lellouch, E., Encrenaz, Th., Bjoraker, G., Samuelson, R., de Graauw, Th., Feuchtgruber, H., Kessler, M.F., 1998. Evidence for water vapor in Titan's atmosphere from ISO/SWS data. *Astron. Astrophys.* 336, L85–L89.

- Crary et al., (in review). Dynamics and composition of plasma at Titan. *Science*.
- Gan, L., Keller, C.N., Cravens, T.E., 1992. Electrons in the ionosphere of Titan. *J. Geophys. Res.* 97, 12,137.
- Hartle, R.E., Killen, R., 2006. Measuring pickup ions to characterize the surfaces and exospheres of planetary bodies: applications to the moon. *Geophys. Res. Lett.* 33 (5), L05201.
- Hartle, R.E., Sittler Jr., E.C., 2004. Pickup ion velocity distributions at Titan: effects of spatial gradients, *EOS Trans. AGU* 85(17), Joint Assembly Suppl., Abstract, P33D-04.
- Hartle, R.E., Sittler Jr., E.C., Ogilvie, K.W., Scudder, J.D., Lazarus, A.J., Atreya, S.K., 1982. Titan's ion exosphere observed from Voyager 1. *J. Geophys. Res.* 87, 1383.
- Hartle, et al., 2006. Preliminary interpretation of Titan plasma interaction as observed by the Cassini plasma spectrometer: comparisons with Voyager 1. *Geophys. Res. Lett.* 33, L08201, doi:10.1029/2005GL024817.
- Keller, C.N., Anicich, V.G., Cravens, T.E., 1998. Model of Titan's ionosphere with detailed hydrocarbon ion chemistry. *Planet. Space Sci.* 46, 1157–1174.
- Ledvina, S.A., Cravens, T.E., 1998. A three-dimensional MHD model of plasma flow around Titan. *Planet. Space Sci.* 46, 1175.
- Ledvina, S.A., Cravens, T.E., Keckskemety, K., 2005. Ion distributions in Saturn's magnetosphere near Titan. *J. Geophys. Res.* 110.
- Lutz, B.L., de Bergh, C., Owen, T., 1983. Titan: discovery of carbon monoxide in its atmosphere. *Science* 220, 1374–1375.
- Michael, M., Johnson, R.E., Leblanc, F., Liu, M., Luhmann, J.G., Shematovich, V.I., 2004. O1\_MRKO1\_MRKEjection of nitrogen from Titan's atmosphere by magnetospheric ions and pickup ions. *Icarus* 175, 263–267.
- Ness, N.F., Acuna, M.H., Lepping, R.P., Connerney, J.E.P., Behannon, K.W., Burlaga, L.F., Neubauer, F.M., 1981. Magnetic field studies by Voyager 1: preliminary results at Saturn. *Science* 212, 211.
- Ness, N.F., Acuna, M.H., Behannon, K.W., Neubauer, F.M., 1982. The induced magnetosphere of Titan. *J. Geophys. Res.* 87, 1369–1381.
- Neubauer, F.M., Gurnett, D.A., Scudder, J.D., Hartle, R.E., 1984. Titan's magnetospheric interaction. In: Gehrels, T., Matthews, M.S. (Eds.), *Saturn*. University of Arizona Press, Tucson, p. 571.
- Owen, T., 1982. The composition and origin of Titan's atmosphere. *Planet. Space Sci.* 30, 833.
- Samuelson, R.E., Maguire, W.C., Hanel, R.A., Kunde, V.G., Jennings, D.E., Yung, Y.-L., Aikin, A.C., 1983. CO<sub>2</sub> on Titan. *J. Geophys. Res.* 88, 8709.
- Sittler, Jr., E.C., Hartle, R.E., Vinas, A.F., Johnson, R.E., Smith, H.T., Mueller-Wodarg, I., 2004. Titan interaction with Saturn's magnetosphere: mass loading and ionopause location. In: *Proceedings of the International Conference TITAN From Discovery to Encounter, 13–17 April 2004, ESTEC, Noordwijk, The Netherlands, SP-1278*, p. 377.
- Sittler Jr., E.C., Hartle, R.E., Viñas, A.F., Johnson, R.E., Smith, H.T., Mueller-Wodarg, I., 2005. Titan Interaction with Saturn's Magnetosphere: Voyager 1 results revisited. *J. Geophys. Res.* 110, A09302.
- Szego, K., et al., 2005. The global plasma environment of Titan as observed by Cassini Plasma Spectrometer during the first two close encounters with Titan. *Geophys. Res. Lett.* 32, L20S05, doi:10.1029/2005GL022646.
- Toublanc, D., Parisot, J.P., Gautier, D., Raulin, F., McKay, C.P., 1995. Photochemical modeling of Titan's atmosphere. *Icarus* 113, 2.
- Waite, et al., 2005. Ion neutral mass spectrometer results from the first flyby of Titan. *Science* 308, 982.
- Young, D.T., et al., 2004. Cassini plasma spectrometer investigations. *Space Sci. Rev.* 114, 1–112.
- Yung, Y.L., 1987. An update on nitrile photochemistry on Titan. *Icarus* 72, 468.
- Yung, Y.L., Allen, Pinto, J.P., 1984. Photochemistry of the atmosphere of Titan: comparison between model and observations. *Astrophys. J. Suppl.* 55, 465.